Multipoint Combined Processing for FMCW LiDAR

Sehun Kim, Yunho Jung, *Senior Member, IEEE*, and Seongjoo Lee, *Senior Member, IEEE*

***Abstract*—This paper proposes a multipoint processing method (MCP) for FMCW LiDAR. The proposed method reduces the number of fast Fourier transform (FFT) calculation compared to the traditional FMCW LiDAR method. This leads to a reduced power consumption. To end this, the proposed method accumulates the multiple beat frequencies in the time domain before the FMCW LiDAR extracts the measured distances from the beat frequencies using the fast Fourier transform (FFT). In order to distinguish the distances that are extracted from the FFT operation, a pulse-width modulation (PWM) counter and an analog comparator were applied. A hysteresis analog comparator was used to increase the immunity from the external noise. When the measured distances are too close to be indistinguishable by the FFT, it may fail to distinguish the measurement order. In order to respond to this situation, the proposed method includes a point-calibration algorithm. The root mean square error (RMSE) and hardware resource usage are utilized in order to assess the performance of the proposed method. The experimental results show that the proposed method achieves power usage time savings compared to the traditional method.**

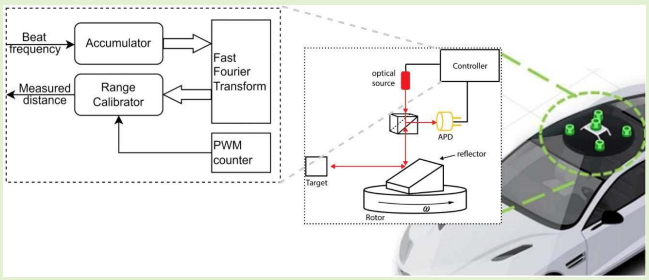

***Index Terms*—LiDAR, FMCW, ADAS.**

I. Introduction

VARIOUS types of heterogeneous sensors are used for advanced driver assistance systems (ADASs) and unmanned aerial vehicles [1]. LiDAR has been used for obstacle detection and intelligent avoidance maneuvers, because it provides accurate distance measurements unlike the general RGB cameras [2]. LiDAR, which is used in various environments such as applications that must be operated by batteries as well as environments in which power can be supplied all the time, is increasing in demand for low-power usage operation. In the unmanned aerial vehicle applications, for example, the LiDAR consuming lower current can increase the flight time of drones. There are two methods that are broadly used for commercial LiDAR applications from smart factory robots to automotive cars [3]. The first method is the full waveform (FW) method, and the other method is the Time-of-Flight (ToF) method [4]. However, these methods are limited by the optical output power and the complexity of the processing units [5]. High-speed analog-to-digital converters and time-to-digital converters are required in order to calculate the distance information, because the range resolution is directly dependent on the sampling rate [6]. The maximum measurable range is dependent on the optical output power. These methods are subject to strict eye safety regulations, because the near-infrared spectrum is used for the output light length [7]. However, the frequency modulated continuous wave (FMCW) method for LiDAR makes it possible to increase the optical output power, because it uses a 1550nm light length [8]. It also mitigates the difficulty of the range resolution improvement, because a lower sampling rate analog-to-digital converter can be used for the FMCW method unlike the full-waveform and the Time-of-Flight methods [9]. With these advantages, the FMCW method will be broadly applied to LiDAR systems in the future. The FMCW LiDAR sensor transmits a chirp signal and receives a reflected signal. Mixing the transmit signal and the received signal produces an IF signal with constant frequency. The frequency (i.e., beat frequency) can be converted into the distance information [10].

$$T_d = \frac{2 \cdot d}{c} \tag{1}$$

$$f_b = \frac{T_d \cdot F_{sweep}}{T_{sweep}} \tag{2}$$

Manuscript received February 8, 2022; accepted March 24, 2022. Date of publication March 31, 2022; date of current version April 29, 2022. This work was supported in part by the Basic Science Research Program through the National Research Foundation of Korea (NRF) funded by the Ministry of Education under Grant 2020R1A6A1A03038540; in part by the NRF funded by the Korean Government (MSIT) under Grant 2020R1A2C1007546; and in part by EDA tools funded by the IC Design Education Center (IDEC), South Korea. The associate editor coordinating the review of this article and approving it for publication was Prof. Piotr J. Samczynski. *(Corresponding author: Seongjoo Lee.)*

Sehun Kim and Seongjoo Lee are with the Department of Information and Communication Engineering & Convergence Engineering of Intelligent Drone, Sejong University, Seoul 05006, South Korea (e-mail: sehun@itsoc.sejong.ac.kr; seongjoo@sejong.ac.kr).

Yunho Jung is with the Department of Smart Drone Convergence, School of Electronics and Information Engineering, Aerospace University, Goyang-si 10540, South Korea (e-mail: yjung@kau.ac.kr).

Digital Object Identifier 10.1109/JSEN.2022.3163740

In Equation (1), T_d is a round-trip delay of the light for the distance (d) where c is the constant of the light. the chirp frequency bandwidth (F_{sweep}) is the difference between the start and stop frequencies of a chirp-modulated signal in Equation (2). The sweep time (T_{sweep}) is the time which is taken for the chirp-modulated signal to reach the stop frequency from the start frequency. The chirp frequency bandwidth and the sweep time are the system parameters. For example, achieving a distance resolution of 3cm requires 5GHz of the bandwidth (F_{sweep}) by Equation (3).

$$d_{res} = \frac{c}{2 \cdot F_{sweep}} \tag{3}$$

When the distance resolution (d_{res}) and the maximum measurable distance (d_{max}) are fixed, the range of f_b depends on the sweep time (T_{sweep}) as like Equation (4).

$$\max(f_b) = \frac{2 \cdot F_{sweep} \cdot d_{max}}{T_{sweep} \cdot c} \tag{4}$$

However, $\max(f_b)$ should be lower than the sampling rate of the Analog-to-Digital Converter (ADC) to capture samples without loss.

$$d = \frac{f_b \cdot T_{sweep} \cdot c}{2 \cdot F_{sweep}} = \frac{T_d \cdot c}{2} \tag{5}$$

The distance (d) from the LiDAR to the target is calculated by Equation (5). Getting the frequency information of the beat frequency needs the FFT processing. The FMCW LiDAR system requires a complex FFT module in order to increase discriminable frequency components [10]. As the FFT point length is increased, the time (T_{fft}), which is consumed by the FFT module, also increased. In the LiDAR system equipped with a low sampling rate ADC, it is desirable to decrease the bandwidth of f_b by increasing the sweep time (T_{sweep}) using Equation (4). However, this causes a poor measurement throughput by increasing the measurement time ($T_{measure}$), which is consumed to measure the distance of an object as like Equation (6).

$$T_{measure} = T_{fft} + T_d + T_{sweep} \tag{6}$$

$$T_{total} = P \cdot T_{measure} \tag{7}$$

To increase measurement throughput (i.e., to decrease $T_{measure}$) without distance resolution loss, it is desirable to decrease the sweep time (T_{sweep}) although a high-speed ADC is required. Equation (7) shows the total measurement time (T_{total}) when the LiDAR measures the distances for P points. In the LiDAR having its parameters as like TABLE I, for example, it should wait for FFT processing to be completed before starting a new distance measurement. Because the FFT processing time (T_{fft}) is a major bottleneck, utilizing multiple FFT modules could be a solution for the bottleneck problem. However, it not only requires a larger silicon area, but it consumes more power. The total power (W_{total}) required to measure the distances P times is calculated using Equation (8).

$$W_{total} = P * (W_{FFT} + W_{optic}) \tag{8}$$

In the LiDAR, there are two major parts. The first part is an optical module, which mainly consists of a laser diode and a photo diode. The power used for the optical part working is W_{optic}. The second part is the Digital Signal Processing (DSP) module, in which a significant amount of power is needed for the FFT module as shown in TABLE II.

TABLE I
AN EXAMPLE OF THE FMCW LIDAR ENVIRONMENT PARAMETERS

Chirp bandwidth (F_{sweep})	5GHz
Range resolution (d_{res})	3cm
Sweep time (T_{sweep})	138us
Maximum distance (d_{max})	100m
FFT point	8192
FFT processing time (T_{fft})	532us

TABLE II
A COMPARISON OF THE POWER CONSUMPTION FOR THE MODULES [11], [12]

W_{optic}	200.0mW
W_{FFT}	221.8mW
W_{ETC}	< 0.1mW

In existing FMCW LiDAR methods, the FFT processing is required for each measurement to obtain the actual distance information, and the FFT processing time (T_{fft}) is a bottleneck for the measurement throughput when the LiDAR continuously takes measurements. Therefore, the total power usage (W_{total}) and the total measurement time (T_{total}) are increased linearly by increasing the number of measurements (P). In this paper, a novel FMCW LiDAR method is proposed to extract the distance information from the beat frequencies with a decreased number of FFT calculations. The proposed method does not extract the distance information through the FFT module for each measurement, but it accumulates a digitized beat frequency signal in the time domain and stores the result in memory. When the number of measurements reaches P, the actual distance information is extracted by working the FFT module. The method can take the measurements for P points with only one FFT calculation. This reduction saves the power to the FFT module as like Equation (9).

$$\hat{W}_{total} = \left(P \cdot W_{optic}\right) + W_{FFT} \tag{9}$$

Because the proposed method does not need to wait until the FFT processing is done, the LiDAR can start to take a new measurement immediately. This improves the measurement throughput by decreasing the total time required for the measurement operation of P points as like Equation (10).

$$\hat{T}_{total} = P \cdot \left(T_d + T_{sweep}\right) + T_{fft} \tag{10}$$

In the FFT processing result, there is no X-axis and Y-axis information of the target, and the result has only the distance information excluding the measurement order. For this reason, constructing a point cloud using only the beat-frequency information can be difficult. In order to mitigate this problem, an analog comparator and a pulse-width modulation (PWM) counter are proposed. The analog comparator detects that an analog beat-frequency signal bounces a threshold level, and

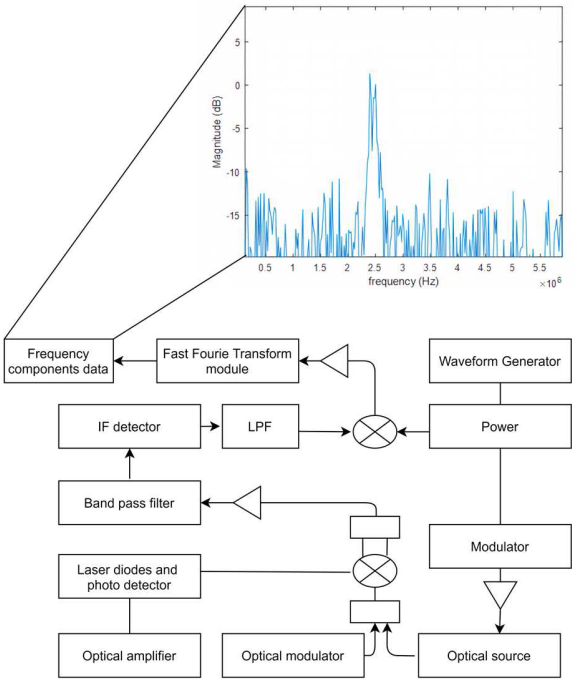

Fig. 1. Traditional FMCW LiDAR architecture [14].

it outputs a high state when the analog signal voltage is higher than the threshold voltage. The PWM counter counts the rising edge of the comparator and stores its value in the measurement order. This information is concatenated with the FFT results in order to obtain the point cloud data. A hysteresis function is applied to the analog comparator, because the analog signal is susceptible to noise. A fluctuation introduced by the noise can affect a large difference in the PWM counter. It is important to select suitable upper and lower hysteresis threshold voltage values in order to minimize the root-mean-square error (RMSE). The hysteresis threshold voltage values were selected based on the simulation results. The simulation program tested all the threshold voltage combinations and collected the RMSE results. After completion, the lowest RMSE was selected using a threshold voltage combination. In this study, in order to verify the improvement of the proposed method, its performance was compared with the performance from the previous study [13].

II. Multipoint Combined Processing Method

Fig. 1 shows a traditional FMCW LiDAR architecture that is based on a previous study [14]. It consists of two major parts. The first is an optical module that converts an electric signal into physical light energy and vice versa. The module includes a laser diode, a photodiode, and an optical modulator. The other is a digital signal processing module that consists of a low-pass filter, a band-pass filter, and a fast Fourier transform processing unit. An FMCW chirp signal, which is created by the waveform generator, was modulated using an optical light source. The modulated signal is transmitted using a laser diode. The beat frequency is extracted by demodulating the chirp signal that is received from the photodetector. The beat frequency is analyzed by the fast Fourier transform module

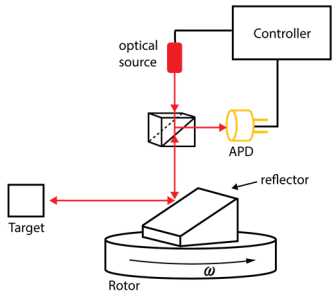

Fig. 2. A MEMS mirror with a rotator for the LiDAR scanner.

in order to obtain the actual distance information [15-16]. Finally, the actual distance information is converted from the beat frequency information that is analyzed by the FFT module using Equation (2). In traditional FMCW LiDAR architecture, the FFT processing should be conducted for each measurement in order to extract the distance information from the LiDAR to a target. In Fig. 1, the spectrum has only one major beat frequency component. This means that the power to operate the FFT module is consumed in order to extract only the frequency component [17].

This means that the power usage increases linearly when the number of measurements is increased. The FMCW LiDAR can measure a fixed position's distance, because it has a single optical module, which is unlike a traditional RGB camera that has multiple optical array cells. A LiDAR is equipped with a scanner in order to measure the distances over a wide area. The scanner is made from a physical actuator using MEMS technology and a rotator. Fig. 2 shows a typical scanner architecture that is used in LiDAR systems. It contains a beam splitter, a micro-mirror, and a rotator in order to manipulate the irradiation angle of a laser diode [18-19]. When the FMCW LiDAR measures distances, the rotator angle information, which is obtained from a Hall effect sensor, is saved into memory with a measurement order. The laser diode emits photons according to the signal input that is generated by an analog front-end module. A photodiode converts the photon strength into an electric current. The optical device and the scanner module, which convert an electrical signal into physical light energy and vice versa, is a spearhead on the FMCW LiDAR system [20]. As a result, the controller obtains the distance information and a rotator angle value. The FMCW LiDAR constructs the point cloud data by converting this information into Cartesian coordinates [20]. Fig. 3 shows a block diagram of the FMCW LiDAR system using the Multipoint Combined Processing (MCP) method. The system consists of a DSP, an analog frontend, and the optic and scanner parts. The analog front-end part preprocesses the signals between the optic and DSP parts. The analog front-end part generates an FMCW chirp signal and modulates it using a phase-locked loop (PLL) and an analog multiplier. A beat frequency signal, which is demodulated from the multiplier, is transferred to the analog-to-digital converter (ADC) and the analog comparator input. The ADC transfers the digitized samples to the adder. The proposed method includes an analog comparator, which is unlike the traditional FMCW LiDAR.

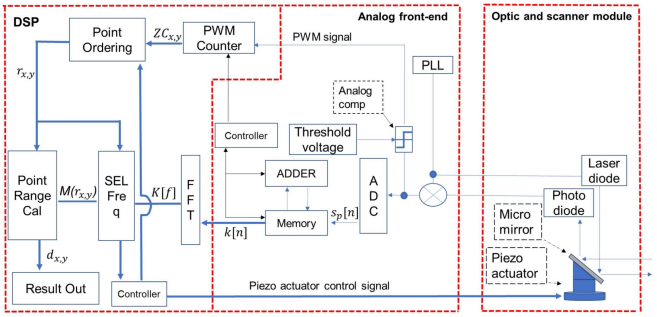

Fig. 3. The proposed method applied FMCW LiDAR system architecture.

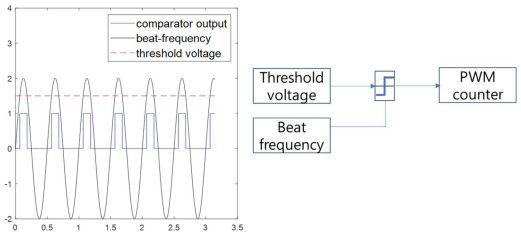

Fig. 4. A waveform of the analog comparator working.

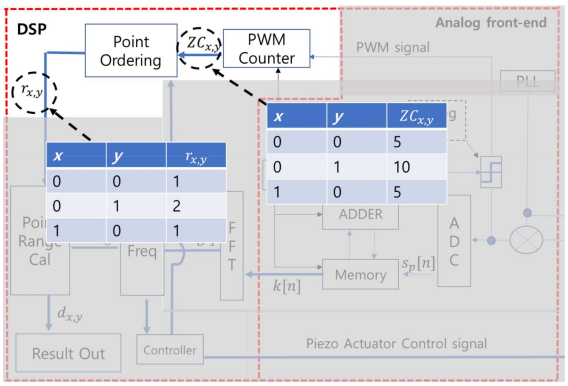

Fig. 5. The PWM counter value ($\boldsymbol{ZC_{x,y}}$) and the rank ($\boldsymbol{r_{x,y}}$) example.

It compares the beat-frequency signal voltage with a reference threshold voltage. When the signal voltage is higher than the upper threshold voltage, the comparator outputs a high state. The output was connected to the PWM counter input in the DSP. The PWM counter counts the rising edge of the comparator output, which is shown in Fig. 4.

Fig. 4 shows an example of a working comparator. The higher the beat frequency, the higher the value of the PWM counter, because the signal crosses the threshold more often. The point-ordering module in the DSP sorts the PWM counter values in an acceding order.

$$r_{x,y} = rank(\boldsymbol{ZC}, ZC_{x,y}) \tag{11}$$

In Equation (11), $ZC_{x,y}$ is the PWM counter value when the scanner coordinates are (x, y). ZC is a set of sizes P with $ZC_{x,y}$ as an element. The $rank(ZC, ZC_{x,y})$ is the rank of the element $ZC_{x,y}$ in ascending order. In order to determine the rank of $ZC_{x,y}$, the values of ZC are sorted in an ascending order and ranked. The result of the point ordering module, $r_{x,y}$ is the rank of the PWM counter values when the scanner's position is (x, y).

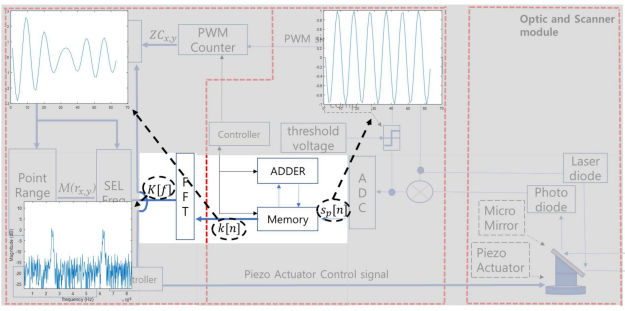

Fig. 6. The beat-frequency adder and an FFT result example.

Algorithm 1 $\widehat{ZC}$ = Sort(**ZC**, max(x), max(y))

Input:

$\boldsymbol{ZC}$ – A set of size P having $ZC_{x,y}$ as an element.
max(x), max(y) – The biggest number of x and y.

Output:

$\widehat{\boldsymbol{ZC}}$ – A set of the sorted $ZC_{x,y}$ in the ascending order.

```
X′=0, Y′=0, x′=0, y’=0 -
WHILE: X′<= max(x),
  Y′=0
  WHILE: Y′<= max(y)
    x′=0
      WHILE: x’< max(x)
      y′=0
        WHILE: y’< max(y)
          IF: ZC_{X′,Y′} > ZC_{x′,y′}
          Swap(ZC_{X′,Y′} and ZC_{x′,y′})
          y′=y′+1
      END
    x′=x′+1
      END
      Y′=Y′+1
  END
  X′=X′+1
END
```

Algorithm 1 shows the pseudocode that is used to sort the set ZC in an ascending PWM counter order. If the counter value of $ZC_{x,y}$ is higher than $ZC_{x,y}$, the values are swapped by the point ordering module in the DSP part. By sorting the set ZC, the sorted set ($\widehat{\boldsymbol{ZC}}$) is ranked according to its value. In Equation (11), the $r_{x,y}$ is the rank of an element ($\widehat{ZC}_{x,y}$) in the set ($\widehat{\boldsymbol{ZC}}$). If there are two or more $ZC_{x,y}$ with the same counter value, they will have the same rank ($r_{x,y}$), which is shown in Fig. 5.

The multipoint combined processing (MCP) method measures the distances P times before the FFT module is working. When each measurement is taken, the beat-frequency samples are accumulated by the adder, and the results are stored in the memory up to P times, which are shown in Fig. 6.

The notation s_p has beat-frequency samples at the p-th measurement in Equation (12) and Fig. 6. The received

signal (s_p) is accumulated with the last received signal until the number of measurements reaches P, in which is illustrated in Equation (12).

$$k[n] = \sum_{p=0}^{P-1} s_p[n] \tag{12}$$

When the number of measurements reaches P, the FFT module in the DSP part starts to work, which is shown in Equation (13), where N is the number of FFT points. The results of the FFT processing are shown in Fig. 6.

$$K[f] = \sum_{n=0}^{N-1} k[n]\, e^{\frac{-j2\pi fn}{N}} \tag{13}$$

After the FFT processing is completed, the frequency selection module in the DSP part selects the local maxima in the frequency spectrum obtained from the FFT module.

$$\boldsymbol{M} = LocalMaxima(|K[f]|) \tag{14}$$

In Equation (14), $K[f]$ has the frequency component values analyzed by the FFT module, and the local maxima ($\boldsymbol{M}$) in the frequency bins ($K[f]$) are extracted using the peak extraction algorithm.

Algorithm 2 $\boldsymbol{M}$ = LocalMaxima($|\boldsymbol{K}[\boldsymbol{f}]$)

INPUT:
$K[f]$ - FFT result
N - FFT length or the size of $\boldsymbol{K}$
OUTPUT:
M– The local maxima of $K[f]$

```
1: i = 1, j = 1, prev_slope=1.0, cur=0, slope=0, prev=0
2: DO
3:    i=i+1
4:    cur= K[i]
5:    slope=cur-prev
6:    IF: cur < prev and prev_slope > 0
7:  M(j)= K[i]
8:  j=j+1
9:    END
10: prev=cur
11: prev_slope=slope
1) WHILE: i < N
```

In Algorithm 2, the local maxima in the frequency bins ($K[f]$) are extracted when a strength of the i-th frequency bin ($K[i]$) is lower than the one that is preceding it ($K[i\text{-}1]$), while the *prev_slope* is a positive value, which means that it is a rising state just before. As a result, the set $\boldsymbol{M}$ has local maxima in an ascending order, and the number of local maxima is num[$\boldsymbol{M}$]. According to Equation (4), the longer the measured distance, the larger the beat frequency, and the higher the beat frequency, the higher the PWM counter value. When two object distances are measured, the PWM counter has counter values for each measurement, and the two local maxima from the beat frequency bins are found by the frequency selection module. However, only one local maximum can be found in the FFT result by the peak extraction algorithm when the target distances are close enough to be indistinguishable by the FFT resolution. In this situation, the number of PWM counter values (num[$\boldsymbol{ZC}$]) and the number of local maxima (num[$\boldsymbol{M}$]) obtained from the FFT processing are different. In order to resolve this situation, the point range calibration module in the DSP part attempts to match between the PWM counter values and the local maxima obtained from the FFT bins. Fig. 7 shows a flowchart of the point-calibration process. The algorithm looks over the PWM counter values ($ZC_{x,y}$) in order to find the two elements with the closest counter value. After the algorithm determines these two elements, it assigns the value of the first element to the other, which results in two elements with equal count values. It iterates as many times as the difference between max($r_{x,y}$) and num[$\boldsymbol{M}$]. After the processing is complete, the PWM counter values ($\boldsymbol{ZC}$) are re-ranked, and the number of ranks equals the number of local maxima.

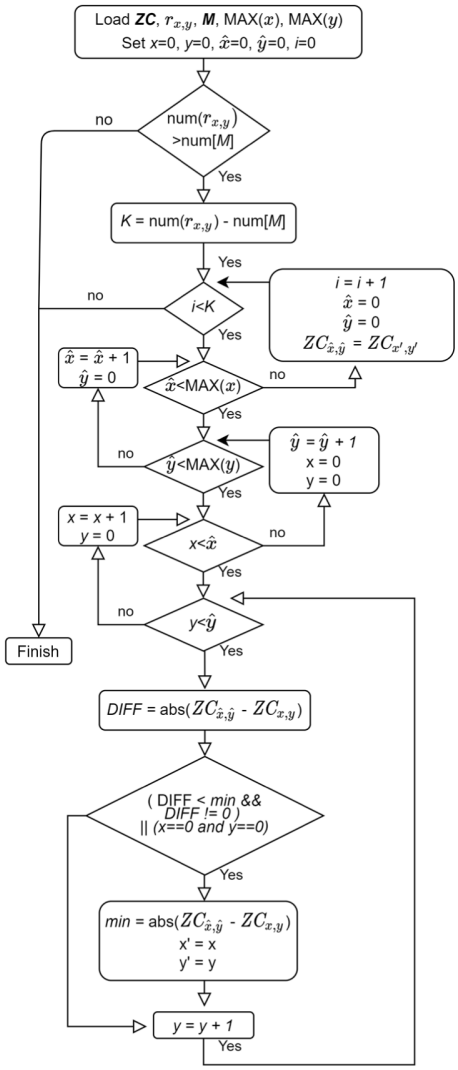

Fig. 7. A flowchart of the point calibration module.

The pairing rank ($r_{x,y}$) and $\boldsymbol{M}$ create a set $M(r_{x,y})$ with the beat-frequency information when the coordinates of the scanner are (x, y). Using Equation (5), the actual distance ($d_{x,y}$)

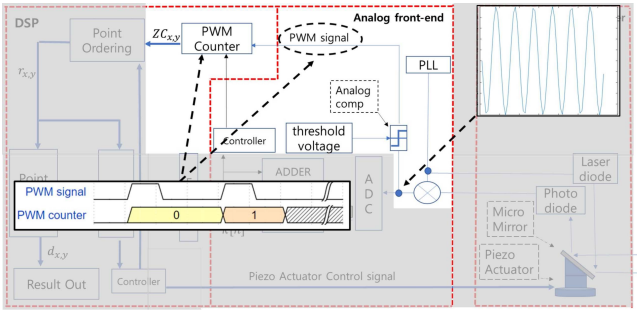

Fig. 8. The analog comparator and the PWM counter working example.

can be converted from the beat frequency using the point range calibration module in the DSP part in Equation (15).

$$d_{x,y} = \frac{M(r_{x,y}) \cdot T_{sweep} \cdot c}{2 \cdot F_{sweep}} \tag{15}$$

The distances of the targets, which are paired with their x and y coordinates, are constructed as a point cloud using this flow. It is the PWM counter value that significantly affects the distance measurement accuracy except when it comes to the distances that are close enough to be indistinguishable by the FFT resolution. If the PWM counter values interfere with the external noise, the ranks of the counter values are changed. This change makes an incorrect pair between $r_{x,y}$ and $K[f]$, which results in a poor RMSE performance. Minimizing the interference from the noise is important in order to minimize the RMSE value. In order to improve the immunity from the external noise, a hysteresis analog comparator is applied to the multipoint combined processing (MCP) method.

III. The PWM Counter Method Combined With the Hysteresis Comparator

The PWM counter module counts the rising edges of the analog comparator output. The analog comparator detects whether the voltage of the received beat frequency signal exceeds a threshold voltage value. When the received signal voltage level exceeds the threshold voltage level, It outputs logic high state. The high-frequency signal voltage value bounces the threshold voltage back and forth more often than a low-frequency signal, so a high PWM counter value means that a high-frequency signal is received.

Fig. 8 shows an example of a PWM counter. The demodulated beat frequency that is obtained from the analog multiplier is transferred to the analog comparator, which is illustrated in Fig. 8. Every time the rising edge of the analog comparator occurs, the value of the PWM counter increases by 1. An analog comparator has only one threshold voltage. However, when a single threshold voltage comparator is used for the PWM counter, the counter value is subjected to external noise. A small amount of noise may cause a vicious effect on the counter value, which results in a higher RMSE value. A hysteresis comparator was used to increase the immunity to the noise [21]. In analog circuits, hysteresis prevents unstable transitions from a comparator by having two threshold levels. In the multipoint combined processing (MCP) method,

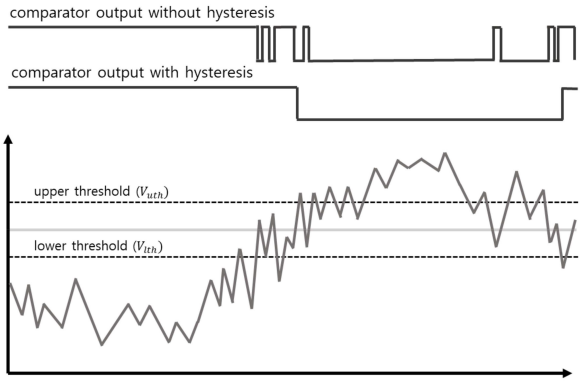

Fig. 9. Hysteresis and non-hysteresis comparison.

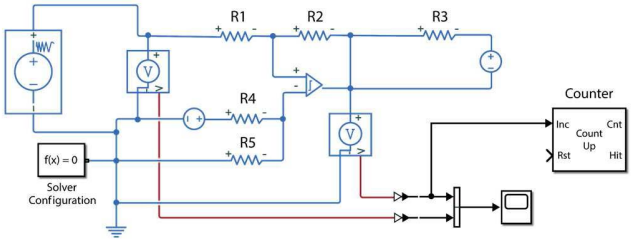

Fig. 10. Hysteresis comparator Simulink circuit model.

a hysteresis comparator is utilized in order to increase the immunity of the comparator from the external noise.

Fig. 9 shows the comparison of the operation of a comparator with hysteresis function and a comparator without hysteresis function for a beat frequency signal mixed with noise from inside or outside. The biggest difference of hysteresis comparator is that it has two threshold values, upper and lower threshold, unlike the non-hysteresis comparator, which has only one threshold value. Unlike the non-hysteresis comparator in which the output of the comparator fluctuates with only a slight error around the threshold due to noise, it can be seen that the hysteresis comparator has considerable immunity to slight noise.

Fig. 10 shows the hysteresis comparator circuit. It has upper and lower threshold voltages. The circuit consists of resistors to create a reference voltage and the threshold levels. The threshold voltages are calculated using Equation (16) and Equation (18).

$$V_{ref} = \frac{VCC \cdot R4}{R4 + R3} \tag{16}$$

$$V_{lth} = \frac{V_{ref} \cdot (R1 + R2)}{R2} \tag{17}$$

$$V_{uth} = \frac{V_{ref} \cdot (R1 + R2) - VCC \cdot R2}{R2} \tag{18}$$

It is important to determine the most suitable threshold voltage level in order to minimize the RMSE value. Hysteresis threshold voltages were determined using simulations. The simulator generates random distances from 10m to 80m for the simulation. The generated distances were converted into beat frequencies using additive white Gaussian noise (AWGN). The adder module accumulates the beat frequencies in the time

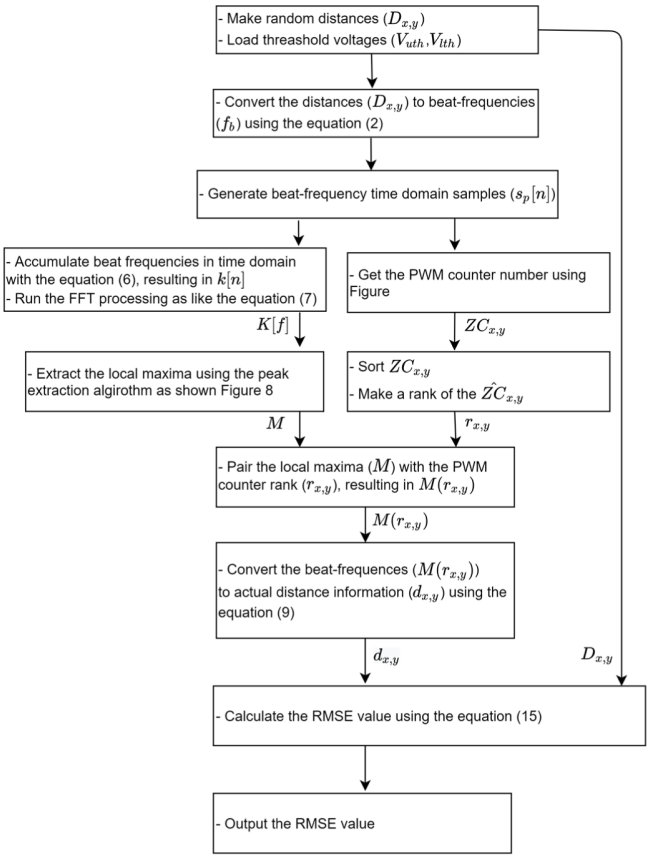

Fig. 11. A flowchart of the *beat_frquency* function in the simulation.

domain. After the accumulation is completed, the FFT module starts to analyze the combined signal. The simulator recovers the distance from the analyzed frequencies using Equation (2), and it calculates the RMSE value. The simulation iterates for all possible threshold voltage combinations. The simulation program determined the threshold voltage combination with the lowest RMSE value for the signal strength change. The threshold voltage varies with 0.1V step from −1V to 1V, while the upper threshold voltage is always higher than the lower threshold voltage. The detailed process of the simulator program is shown in Algorithm 3 and Fig. 11.

Algorithm 3

OUTPUT: *RMSE* – root mean square error of the system at V_{uth}, V_{lth}
1: V_{lth}=-1.0, V_{uth}=-0.9
2: DO
3: V_{uth}=V_{lth}+0.1
4: DO
5: *RMSE*= beat_frequency(V_{uth}, V_{lth})
6: WHILE: V_{uth}<=1.0
7: WHILE: V_{lth}<0.9

Algorithm 3 shows how the simulator works for all threshold voltage combinations. The threshold values (V_{uth}, V_{lth}) are initialized with -1V and -0.9V. The initialized threshold

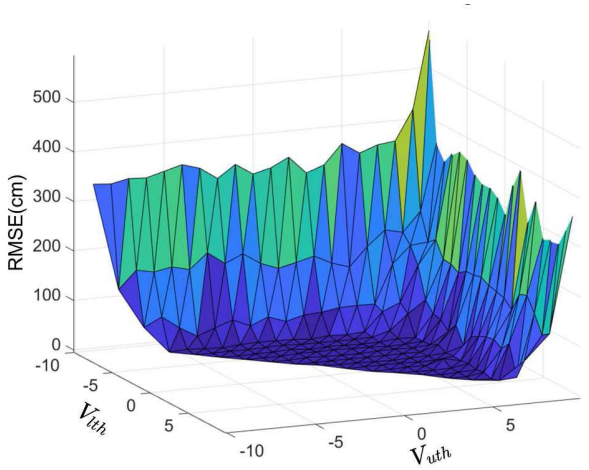

Fig. 12. RMSE result for the threshold combinations.

voltages are transferred to the beat_frequency function, which returns the RMSE value, which is shown in Algorithm 3. In Fig. 11, the *beat_frequency* function in the simulation, the load threshold voltages (V_{uth}, V_{lth}) for the analog comparator, and the simulator program generate a random distance value ($D_{x,y}$) to be simulated. The random distance ranged from 10 m to 80 m. The generated distances are used for the RMSE calculation at the end of the simulation process, and the distances ($D_{x,y}$) are converted to a beat-frequency signal (f_b) using Equation (2). The time-domain beat-frequency signal samples ($s_p[n]$) are compared with the threshold voltages (V_{uth}, V_{lth}) of the hysteresis comparator that results in the PWM counter value ($ZC_{x,y}$), which is shown in Fig. 5. The PWM counter value is replaced with the rank ($r_{x,y}$) by the sorting and rank decision, which is shown in Algorithm 1 and Equation (5). Meanwhile, the time domain samples ($s_p[n]$) are also accumulated by the adder, and the accumulated signal ($k[n]$) is used to extract the frequencies ($K[f]$) using fast Fourier transform (FFT) processing. The local maxima ($\boldsymbol{M}$) of the frequencies are selected from the beat-frequency information ($K[f]$) using Algorithm 2, and the local maxima ($\boldsymbol{M}$) and the PWM counter rank ($r_{x,y}$) are calibrated, which are shown in Fig. 7. When the number of local maxima is equal to the largest number of ranks ($\max(r_{x,y})$), the local maxima ($\boldsymbol{M}$) and the PWM counter rank ($r_{x,y}$) are paired, which results in $\boldsymbol{M}(r_{x,y})$, and it is the local maximum value according to the PWM counter's rank when the coordinates of the LiDAR scanner are x and y. The extracted and paired beat frequencies are converted to the distance information ($d_{x,y}$) using Equation (2). Finally, the randomly generated original distances ($D_{x,y}$) and the recovered distances ($d_{x,y}$) from the beat frequencies were calculated in order to obtain the RMSE result using Equation (19). These processes, which are shown in Fig. 11, are repeated as many times as the number of all threshold combinations in order to find the smallest RMSE value, which are shown in Algorithm 3.

Fig. 12 shows the RMSE results that were obtained from the simulations. There were changes in the RMSE values according to threshold variation. The simulation results show

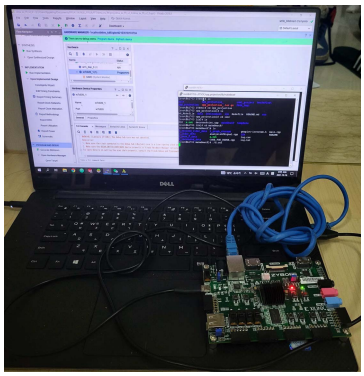

Fig. 13. FPGA configuration and test of the system.

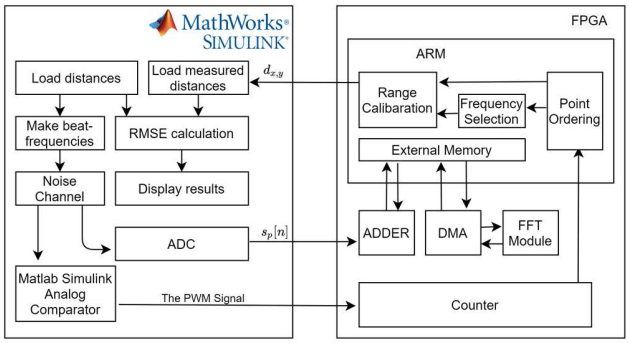

Fig. 14. Verification environments.

TABLE III
VERIFICATION ENVIRONMENT PARAMETER

Chirp bandwidth	5GHz
Range resolution	3cm
Clock speed	100MHz
Sweep time	138us
Processing time	532us
RMSE	0.15cm
FFT point	8192

the lowest RMSE value at 0.7V for the upper threshold voltage (V_{uth}) and -0.5V for the lower threshold voltage (V_{lth}).

IV. Simulation and Verification Results

The performance comparison of the proposed system with the other system was conducted using Xilinx XC7Z020, which is a field programmable grid array (FPGA), and MATLAB Simulink, which is shown in Fig. 13. The analog frontend, which includes a noise channel and analog comparators, was emulated using MATLAB Simulink [22]. The FPGA includes the digital signal processing (DSP) part of the proposed system, which includes the pre-made digital IPs. It consists of a direct memory access (DMA) and an FFT IP, which are shown in Fig. 14.

The PWM counter in the FPGA counts the pulses that are generated by an analog comparator in MATLAB Simulink. In Fig. 14, the FFT module starts to work after the adder module completes the accumulation of the beat frequency samples, while the PWM counter counts the rising edges from the PWM signal. The point-ordering module sorts the PWM counter values and ranks them as sorted counter values. The frequency-selection module determines the local maxima from the FFT results. Finally, the range calibration module starts the pairing between the PWM counter rank and the local maxima of the beat frequencies. After the range calibration was completed, the measured distance ($d_{x,y}$) was transferred to MATLAB Simulink in order to compare the original distance and the measured distance. Simulink calculates the RMSE with the original distance ($D_{x,y}$) and the measured distance ($d_{x,y}$) by using Equation (15).

TABLE III lists the specifications of the verification environment. The FFT and DMA IP operate at 100MHz. The FMCW chirp frequency bandwidth was 5GHz, and an 8192-points FFT was used. The theoretical range resolution (d_{res}) was 3cm according to Equation (3).

$$RMSE = \sqrt{\frac{1}{P}\sum_{p=0}^{P-1}(d_{x,y} - D_{x,y})^2} \tag{19}$$

In this study, in order to show how the RMSE performance changes depending on multiple parameters, a simulation was conducted on multiple distances, multiple signal strengths, and variation of the number of combined beat frequencies. The experiment was performed under the following conditions, which four targets were applied. The positions of the targets were located at 10, 20, 40, and 80m. The signal strength was tested under two conditions, which included 40 and 80dB. In the proposed method, the number of combined beat frequencies was tested for five cases, which included 5, 10, 15, 20, and 25. For a performance comparison with the previous studies, the RMSE result table includes the single-point FMCW LiDAR method results [13]. A total of 1500 experiments were repeated in each case in order to calculate the RMSE using Equation (15). TABLE IV - V shows the RMSE performance results of the Multipoint Combined Processing (MCP) method and the traditional single-point FMCW LiDAR methods at signal strengths that ranged from 40dB to 80dB. The traditional single-point methods [13][14] are based on Fig. 1 which extract the distance information from the spectrum including one beat frequency component only. The experimental parameters of the traditional methods are also based on TABLE III (but Kim's method uses 256-point FFT). The MCP method shows a poor RMSE performance compared to the single-point FMCW LiDAR method when the signal power is 40dB, which is shown in TABLE IV. The RMSE result of the conventional method, which had the largest RMSE value in the single-point method, was 15.25cm, whereas RMSE result of the MCP method was significantly larger than the result of the single-point method for all the measurement distances. The hysteresis analog comparator is used to increase the immunity of the received signal against an external noise. However, the PWM counter has the possibility of creating an error, which results in a chaotic ranking of the PWM counter values when the signal power is low. If the signal strength of the beat frequency is low, the point select module of the DSP part will select the

TABLE IV
RMSE(cm) RESULT FOR SIGNAL STRENGTH 40dB

Distance / num*	MCP					SP **	
	10m	20m	40m	80m	Average	Kim et al. [13]	Gao et al. [14]
5	22.36	132.58	63.63	60.55	90.34	9.0	15.25
10	119.59	117.24	34.51	77.74	98.96		
15	19.35	147.68	115.57	107.88	97.12		
20	5.36	93.80	144.15	3.35	57.65		
25	25.56	112.26	119.94	141.40	81.26		

* The number of accumulated frequencies ** Single Point FMCW LiDAR

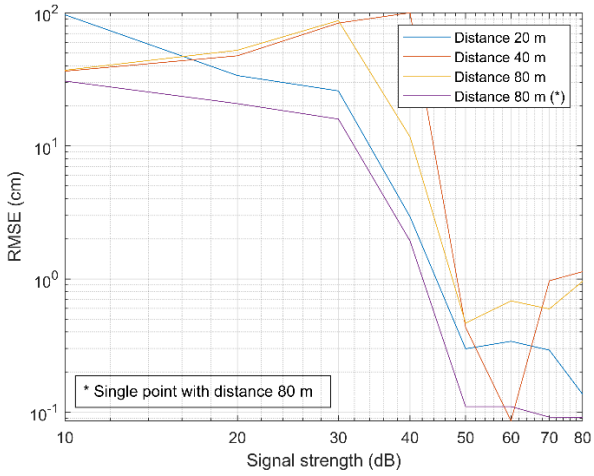

Fig. 15. The RMSE variation of the MCP method when the number of cumulative beat frequency is 15.

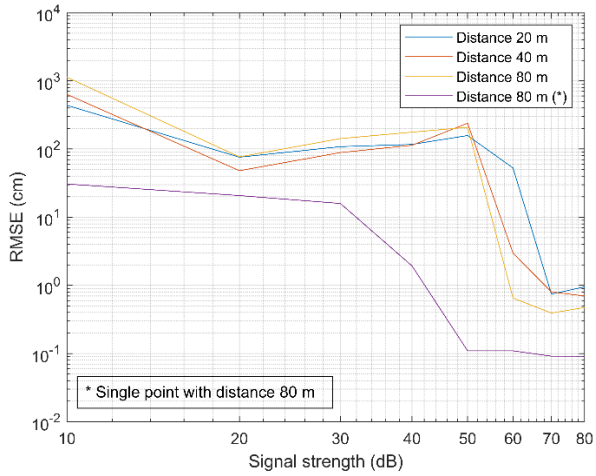

Fig. 16. The RMSE variation of the MCP method when the number of cumulative beat frequency is 25.

incorrect local maximum in the frequency spectrum. However, when the signal strength of the beat-frequency is 80dB, the RMSE is decreased up to 0.15cm when the measurement target distance is 20m. It was confirmed that the RMSE performance improved as the signal strength increased, which is shown in TABLE IV - V. However, the RMSE performance tended to gradually deteriorate as the number of combined points (num*) increased, even though the received signal strength increased to 80dB, which is shown in TABLE V. This is because the greater the number of combined beat frequencies, the higher the probability that a small distance difference was measured than the FMCW measurement precision. The FMCW LiDAR can have a relatively strong signal strength, because it can use a stronger light output. However, the number of beat frequencies to be combined in the system is determined by the experimental results. Fig. 15 and Fig. 16 show the RMSE variation of the multipoint combined processing method with the beat frequency signal strength change. The number of combined beat frequencies was 15 and 25. The beat frequency signal strength ranged from 10dB to 80dB with a target distance of 20, 40, and 80m which is shown in Fig. 15 - Fig. 16.

In Fig. 15, when the number of combined beat frequencies is 15, the RMSE starts to decline sharply at the beat frequency signal strength of 30 dB. However, when the number of combined beat frequencies is 25, the RMSE started to decrease from 50 dB as shown in Fig. 16. This is because a noise makes the rank of the PWM counter value ($r_{x,y}$) and the local maxima ($\boldsymbol{M}$), which are obtained from the point ordering module of the DSP part, incorrectly matched one another. The multipoint combined processing method used in the experiment uses the 8192-point FFT module. In a previous study, which reduced the hardware complexity by reducing the number of FFT points through the digital down converter (DDC) technique, a 256-point FFT was used [13]. In this study, the beat frequency is extracted using multiple operations of the FFT module. With these properties, the hardware complexity comparison between the proposed method and the traditional single-point processing method shows that the proposed method has twice the complexity of the traditional method. However, when it comes to the processing time for the multiple measured distances, the multipoint combined processing method takes the same amount of time as the single point processing (SP) method in order to extract distance information, because the proposed method processes multiple beat frequencies simultaneously. As the traditional single-point FMCW LiDAR method can extract the distance from the beat frequency for each measurement, the FFT processing time increases depending on the number of measurements. TABLE VI shows the results of comparing the processing time that is required to extract the actual distance between the traditional method and the

TABLE V
RMSE(cm) RESULT FOR SIGNAL STRENGTH 80dB

Distance / num*	MCP					SP **	
	10m	20m	40m	80m	Average	Kim et al. [13]	Gao et al. [14]
5	1.22	0.80	0.48	0.51	0.76	3.0	0.12
10	0.52	0.15	0.55	0.44	0.38		
15	0.63	0.51	1.11	0.81	0.64		
20	1.05	1.12	0.32	1.08	0.78		
25	1.18	1.41	0.65	0.49	0.83		

* The number of accumulated frequencies ** Single Point FMCW LiDAR

TABLE VI
COMPARISON OF PROCESSING TIME USAGE

Points	Total FFT processing time @ 100MHz	
	MCP	SP (Kim *et al*. [13])
5	532us	856us
10		1712us
15		2568us
20		3424us

TABLE VII
COMPARISON OF HARDWARE RESOURCE USAGE

Resource utilization (XC7Z020)			
LUTs		Flip-Flops	
MCP	Kim *et al* [13].	MCP	Kim *et al* [13].
1374	661	2440	1059

new method when the distances were measured from 5 to 20 with intervals of 5 each, which takes 3.4 milliseconds, and the MCP takes only 0.5 milliseconds. The multipoint combined processing method has a disadvantage in terms of time complexity compared to the traditional LiDAR method, which assumes that only one distance is measured, because the actual distances can be extracted by executing the FFT module with a complexity of 8192-points at least once in the multi-point combined processing method even for a single measurement. However, when measuring the distance of multiple measurement points in order to create a point cloud, the MCP method, which does not perform an FFT operation for every measurement, is superior in terms of the time complexity.

TABLE VII shows the hardware complexity comparison between the proposed method (MCP) and the traditional method (SP). In both cases of LUT and flip-flop, the proposed method required twice as many hardware resources as the conventional method, because the proposed method includes the adder and PWM counter.

V. CONCLUSION

In this paper, a multipoint combined processing method for FMCW LiDAR is proposed to decrease the number of FFT calculation. The main idea is to accumulate the received beat frequency in the time domain. Unlike the traditional single-point FMCW LIDAR method, which had to activate the FFT module for each measurement in order to extract the distance information from the beat frequency signal, the proposed method, which accumulates the beat frequencies in the time domain, can extract multiple distances with one FFT operation. The frequency spectrum obtained from the FFT operation does not have the coordinate information of the LiDAR scanner, so the proposed method introduces an analog comparator and a PWM counter. They were used to compose the point cloud data by matching the extracted distance with the x and y coordinates of the LiDAR scanner. The beat frequency in the analog state that is not sampled by the ADC is vulnerable to external noise. In particular, when the voltage of the beat frequency signal swings close to the analog comparator threshold, the value of the PWM counter has a significant amount of error. In this study, a hysteresis comparator was used to increase the immunity from external noise. The hysteresis analog comparator has two thresholds and a hysteresis function, so it can mitigate the malfunction of the PWM counter, which is due to noise in the signal. Nevertheless, if the strength of the received signal is weak, the analog comparator will be subjected to noise, which results in an incorrect value of the PWM counter. Consequently, an incorrect PWM counter increases the RMSE. This phenomenon was confirmed through the simulation results when the signal strength of the beat frequency was 40dB and 80dB. Comparing the proposed method with Kim *et al.* shows that as the number of combined points increases, the MCP technique significantly reduces the time required for an FFT operation.

REFERENCES

[1] A. Geiger, P. Lenz, and R. Urtasun, "Are we ready for autonomous driving? The KITTI vision benchmark suite," in *Proc. IEEE Conf. Comput. Vis. Pattern Recognit.*, Jun. 2012, pp. 3354–3361, doi: 10.1109/CVPR.2012.6248074.

[2] A. Rangesh and M. M. Trivedi, "No blind spots: Full-surround multi-object tracking for autonomous vehicles using cameras and LiDARs," *IEEE Trans. Intell. Vehicles*, vol. 4, no. 4, pp. 588–599, Dec. 2019, doi: 10.1109/TIV.2019.2938110.

[3] J. Martin, S. May, S. Endres, and I. Cabanes, "Decentralized robot-cloud architecture for an autonomous transportation system in a smart factory," in *Proc. SEMANTICS Workshops*, 2017, pp. 1–8.

[4] D. Li *et al.*, "Co-path full-waveform LiDAR for detection of multiple along-path objects," *Opt. Lasers Eng.*, vol. 111, pp. 211–221, Dec. 2018.

[5] E. Gregorio, F. Rocadenbosch, R. Sanz, and J. Rosell-Polo, "Eye-safe lidar system for pesticide spray drift measurement," *Sensors*, vol. 15, no. 2, pp. 3650–3670, Feb. 2015.
[6] B. Behroozpour, P. A. M. Sandborn, M. C. Wu, and B. E. Boser, "Lidar system architectures and circuits," *IEEE Commun. Mag.*, vol. 55, no. 10, pp. 135–142, Oct. 2017, doi: 10.1109/MCOM.2017.1700030.
[7] M. E. Warren, "Automotive LIDAR technology," in *Proc. Symp. VLSI Circuits*, Jun. 2019, pp. C254–C255, doi: 10.23919/VLSIC.2019.8777993.
[8] H. K. Tsang *et al.*, "Two-photon absorption and self-phase modulation in InGaAsP/InP multi-quantum well wave-guides," *J. Appl. Phys.*, vol. 70, no. 7, pp. 3992–3994, 1991.
[9] K. Yoshioka *et al.*, "A 20ch TDC/ADC hybrid SoC for 240×96-pixel 10%-reflection <0.125%-precision 200 m-range imaging LiDAR with smart accumulation technique," in *IEEE ISSCC Dig. Tech. Papers*, Feb. 2018, pp. 92–94, doi: 10.1109/ISSCC.2018.8310199.
[10] E. Hyun and J.-H. Lee, "Method to improve range and velocity error using de-interleaving and frequency interpolation for automotive FMCW radars," *Int. J. Signal Process., Image Process. Pattern Recognit.*, vol. 2, no. 2, pp. 11–21, 2009.
[11] G. Zhang *et al.*, "Demonstration of high output power DBR laser integrated with SOA for the FMCW LiDAR system," *Opt. Exp.*, vol. 30, no. 2, pp. 2599–2609, 2022.
[12] M. Liu, P. Zhao, T. Wu, K. K. Parhi, X. Zeng, and Y. Chen, "A low-power twiddle factor addressing architecture for split-radix FFT processor," *Microelectron. J.*, vol. 117, Nov. 2021, Art. no. 105276.
[13] C. Kim, Y. Jung, and S. Lee, "FMCW LiDAR system to reduce hardware complexity and post-processing techniques to improve distance resolution," *Sensors*, vol. 20, no. 22, p. 6676, Nov. 2020.
[14] S. Gao and R. Hui, "Frequency-mFrequency-modulated continuous-wave lidar using I/Q modulator for simplified heterodyne detection," *Opt. Lett.*, vol. 37, no. 11, pp. 2022–2024, 2012.
[15] F. Ali and M. Vossiek, "Detection of weak moving targets based on 2-D range-Doppler FMCW radar Fourier processing," in *German Microw. Conf. Dig. Papers*, Mar. 2010, pp. 214–217.
[16] S. Kameyama, T. Ando, K. Asaka, Y. Hirano, and S. Wadaka, "Performance of discrete-Fourier-transform-based velocity estimators for a wind-sensing coherent Doppler lidar system in the Kolmogorov turbulence regime," *IEEE Trans. Geosci. Remote Sens.*, vol. 47, no. 10, pp. 3560–3569, Oct. 2009, doi: 10.1109/TGRS.2009.2022062.
[17] J. Lee, Y.-A. Li, M.-H. Hung, and S.-J. Huang, "A fully-integrated 77-GHz FMCW radar transceiver in 65-nm CMOS technology," *IEEE J. Solid-State Circuits*, vol. 45, no. 12, pp. 2746–2756, Dec. 2010, doi: 10.1109/JSSC.2010.2075250.
[18] D. Wang, C. Watkins, S. Koppal, M. Li, Y. Ding, and H. Xie, "A compact omnidirectional laser scanner based on an electrothermal tripod MEMS mirror for lidar," in *Proc. 20th Int. Conf. Solid-State Sens., Actuators Microsyst. Eurosensors XXXIII (TRANSDUCERS EUROSENSORS XXXIII)*, Jun. 2019, pp. 1526–1529, doi: 10.1109/TRANSDUCERS.2019.8808659.
[19] X. T. Nguyen, V. L. Dinh, H.-J. Lee, and H. Kim, "A high-definition LIDAR system based on two-mirror deflection scanners," *IEEE Sensors J.*, vol. 18, no. 2, pp. 559–568, Jan. 2018, doi: 10.1109/JSEN.2017.2777500.
[20] T. Fersch, R. Weigel, and A. Koelpin, "Increasing the signal-to-noise ratio in APD-based scanning LiDAR sensors on the transmission side," in *Proc. IEEE Conf. Recent Adv. Lightw. Technol. (CRALT)*, Sep. 2016, pp. 1–3, doi: 10.1109/CRALT.2016.8066038.
[21] A. Raj, S. Y. Divvela, G. Singh, and S. Kundu, "Trade-off characteristics of hysteresis comparator used in noisy systems," in *Proc. Devices Integr. Circuit (DevIC)*, Mar. 2019, pp. 413–417, doi: 10.1109/DEVIC.2019.8783668.
[22] *MATLAB and Simulink Release*, MathWorks, Natick, MA, USA, 2012.

Sehun Kim received the B.S. dual degree in electrical engineering and computer science from Sejong University, in 2020. He is currently pursuing the M.S. degree in information and communication engineering and convergence engineering of intelligent drones. His research interests include LUNA (data science and computer graphics method).

Yunho Jung (Senior Member, IEEE) received the B.S., M.S., and Ph.D. degrees in electrical and electronic engineering from Yonsei University, Seoul, South Korea, in 1998, 2000, and 2005, respectively. From 2005 to 2007, he was a Senior Engineer with the Telecommunication Network Division, Communication Research Center, Wireless Device Solution Team, Samsung Electronics Company Ltd., Suwon, South Korea. From 2007 to 2008, he was a Research Professor with the Institute of TMS Information Technology, Yonsei University. He is currently a Professor with the School of Electronics and Information Engineering, Korea Aerospace University, Goyang, South Korea. His current research interests include signal processing algorithm and system on-chip (SoC) implementation for radars, wireless communications, and image processing systems.

Seongjoo Lee (Senior Member, IEEE) received the B.S., M.S., and Ph.D. degrees in electrical and electronic engineering from Yonsei University, Seoul, South Korea, in 1993, 1998, and 2002, respectively. From 2002 to 2003, he was a Senior Research Engineer with the IT SOC Research Center and the ASIC Research Center, Yonsei University. From 2003 to 2005, he was a Senior Engineer at Core Tech Sector, Visual Display Division, Samsung Electronics Company Ltd., Suwon, South Korea. He was a Research Professor with the IT Center and the IT SoC Research Center, Yonsei University, from 2005 to 2006. He is currently a Professor with the Department of Information and Communication Engineering, Sejong University, Seoul. His current research interests include system-on-chip (SoC) designs for wireless communication systems, RADAR and LiDAR signal processing, and SoC designs for image signal processing.